Available online at www.sciencedirect.com
SCIENCE DIRECT®
International Journal of Heat and Mass Transfer 49 (2006) 3702–3707
International Journal of HEAT and MASS TRANSFER
www.elsevier.com/locate/ijhmt

Experimental and RDFI calculated radiative properties of a mullite foam

Barbar Zeghondy, Estelle Iacona *, Jean Taine

Laboratoire EM2C, École Centrale Paris, Grande Voie des Vignes – 92295 Châtenay Malabry, France

Received 12 October 2005; received in revised form 9 February 2006
Available online 18 May 2006

Abstract

The solid phase of a mullite foam has been experimentally characterized as a mainly scattering semi transparent medium with an isotropic phase function. In a second step, from the corresponding determined data, the Radiative Distribution Function Identification (RDFI) method of Zeghondy et al. has been applied to predict the bi-directional reflectance of a mullite foam sample. A direct experimental determination of this reflectance agrees with the model results.

Keywords: Bi-directional reflectance and transmittance; Scattering; Porous medium

1. Introduction

The knowledge of the radiative properties of porous media, considered as semi transparent, is a key point for solving many types of radiative transfer problems. In this section, we mainly consider foams or ceramics. The radiative properties have been, in the most cases, identified from measurements. For this type of media, Kamiuto [1] has developed a least-square method to solve an inverse scattering problem to identify the optical thickness, the albedo and the asymmetry factor of an assumed Henyey–Greenstein phase function. The model has been applied to corderite and to Ni–Cr porous plates [2] and to a dispersed medium bounded by transparent plates [3]. Glicksman et al. [4] have measured the directional transmissivity of foam and glass fiber by using a CO_2 laser and identified absorption and extinction coefficients and phase function from simple solutions of the RTE equation. Hendricks and Howell [5,6] have obtained spectral radiative properties of high porosity ceramics from spectral hemispherical reflectance and transmittance measurements, by using an inverse analysis technique based on a discrete ordinate radiative model. They have also developed an original radiative analysis approach applied to reticulated porous ceramics [7]. The direct transmittance is treated separately from the transmittance issued from interactions with internal structures. Baillis–Doermann et al. [8–11] have carried out similar works for open cell foam insulation. Other references are given in two reviews [12,13].

The present paper deals with the experimental characterization of mullite foam radiative properties and presents, for this foam, an experimental validation case of the Radiative Distribution Function Identification (RDFI) method. This approach, initially developed by Tancrez and Taine [14], is detailed in Zeghondy et al. [15]. It leads to the radiative properties of a high porosity medium, modeled as semi transparent, only from both morphological data issued from an X-ray tomography and local radiative properties of its solid phase. These local properties are characterized by porosity scales smaller than the tomography spatial resolution. Three steps are considered: (i) the experimental determination of $\kappa_{\nu S}(\mathbf{u})$ and $\beta_{\nu S}(\mathbf{u})$, absorption and extinction coefficients of a solid phase sample (mullite) in Section 3; the associated phase function is discussed. These data have been used in Ref. [15]; (ii) the experimental determination of the bi-directional reflectance of a mullite foam

* Corresponding author. Tel.: +33 141131075; fax: +33 147028035.
E-mail address: estelle.iacona@em2c.ecp.fr (E. Iacona).

0017-9310/$ - see front matter © 2006 Elsevier Ltd. All rights reserved.
doi:10.1016/j.ijheatmasstransfer.2006.02.036

sample in Section 4.1. The experimental setup and the procedure in use in Sections 3 and 4.1 are detailed in Section 2; (iii) a comparison in Section 4.2 between data of (ii) and the corresponding bi-directional reflectance data calculated from both the radiative properties of the mullite foam obtained in Ref. [15] and from a Monte Carlo transfer model.

2. Experimental setup and procedure

This section presents the experimental setup and procedure used to measure: (i) the bi-directional reflectance of both a porous medium sample and a sample made of this porous medium solid phase; (ii) the bi-directional transmittance of this last sample.

2.1. Experimental setup

The optical setup designed to measure the bi-directional reflectance and transmittance of a sample, limited to the incidence plane, is described in Fig. 1, and detailed by Greffet and Ladan [16]. The sample is accurately fixed on a rotary support, which allows us to change the incident angle θ_i. The source is an expansed He–Ne laser beam, of wavelength 632.8 nm and of 8 mm diameter. A lock-in amplifier technique is used to eliminate radiation issued from other sources. The laser beam passes through a chopper. It is then divided by a beam splitter into two parts. The signal S_1 associated with the reflected beam is measured by a photodiode PD to take into account the laser intensity fluctuations. The transmitted beam impacts the sample. The detection elements are set up on a motorized rotary arm. The beam is collected by a 28 mm diameter and 50 mm focal lens, which focuses it in a photomultiplier PM, which leads to a signal S_2. The photodiode detection surface is defined by a 0.5 mm diameter diaphragm, which corresponds to an elliptic object area of 6 mm small axis on the sample surface. The solid angle $\Delta\Omega_d$ of light collection

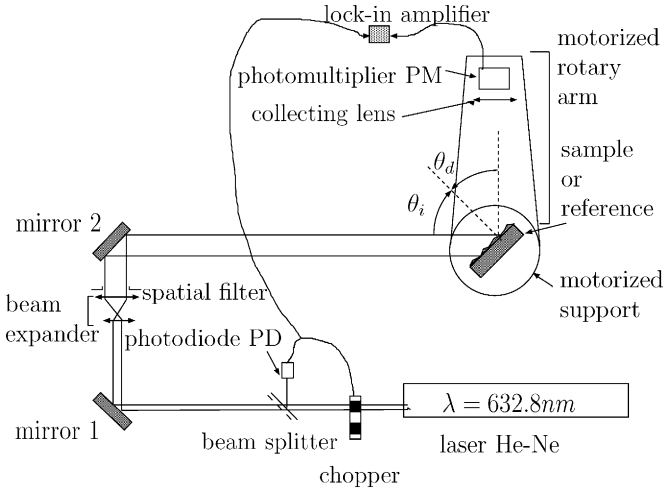

Fig. 1. Transmittance and reflectance measurement setup.

by the PM is 0.0027 sr. The associated half angle is 1.8°. Both signals S_1 and S_2, received by the photodiode and the photomultiplier, are treated by the lock-in amplifier which gives S_2/S_1. The detection angle θ_d is practically limited by mechanical elements of the set up. Its useful variation range is typically 60°. As the entire setup is motorized, measurements can be carried out with different incidence and detection angles θ_i and θ_d. The accuracy on θ_i and θ_d is 0.01°.

2.2. Samples and reference

Two kinds of samples are considered (EcoCeramics, The Netherlands).

The first sample is a mullite foam of porosity Π close to 0.85, also characterized by the RDFI method in Ref. [15]. It is a rectangular plate of 50 mm edge and 12 mm thickness, characterized by three scales of porosity. The two smallest ones have been determined by a mercury porosimetry as shown in Fig. 5 of Ref. [15]. The corresponding typical pore sizes are 1 and 40 μm. The largest pore size, not determined by a mercury porosimetry technique, is 300 μm. As the three ranges of the pore distribution do not overlap, three partial porosities 0.40, 0.11 and 0.34 can be crudely associated with the typical pore sizes 1, 40 and 300 μm, respectively. The two largest pore sizes are taken into account in the RDFI approach of Ref. [15].

The knowledge of the foam solid phase radiative properties, only including the effects of the 1 μm pores, is required in this model. Consequently, a second sample made of the foam solid phase has been experimentally studied. It is called, in the following, mullite sample. After a large number of tests, it was not possible, due to the material fragility, to obtain sample thickness smaller than 0.25 mm which corresponds to a very large optical thickness (of 26 from Eq. (6)). Its surface roughness is characterized by the 1 μm pore size.

The reference material, defined in Section 2.1, is characterized by a diffuse bi-directional reflectivity and an hemispherical spectral reflectance of 0.85 [16].

2.3. Experimental procedure

The useful part of the incident flux is given by

$$\mathrm{d}\Phi^i_{vA} = \langle I^i_v \rangle \cos\theta_i \Delta\Omega_I \Delta v \int_A f(x,y)\,\mathrm{d}x\,\mathrm{d}y \tag{1}$$

where $\langle I^i_v \rangle$ is the mean intensity of the laser, Δv ($\simeq 10^3$ cm^{-1}) its width in frequency, $\Delta\Omega_I$ ($\simeq 10^{-8}$ sr) the solid angle of the expansed beam; A the elliptic surface conjugated object of the detection diaphragm surface; $f(x,y)$ the distribution function of the laser intensity in A. The flux detected by the photomultiplier is

$$\mathrm{d}\Phi^d_{vA}(\theta_i,\theta_\mathrm{d}) = \mathrm{d}\Phi^i_{vA} R''_v(\theta_i,\theta_\mathrm{d}) \cos\theta_\mathrm{d} \Delta\Omega_\mathrm{d} \tag{2}$$

assuming that R''_v, the bi-directional reflectance of the sample or the reference is uniform within each solid angle $\Delta\Omega_\mathrm{d}$

and on the surface A. In practice, the ratios $d\Phi^{d}_{\nu samp}/d\Phi^{d}_{\nu ref}$ and $d\Phi^{PD}_{\nu samp}/d\Phi^{PD}_{\nu ref}$ are used to eliminate the fluctuations of the laser intensity where $d\Phi^{PD}_{\nu ref}$ and $d\Phi^{PD}_{\nu samp}$ are the fluxes reflected by the beam splitter and detected by the photodiode for the reference and the sample respectively. The sample bi-directional reflectance is

$$\frac{R''_{\nu samp}(\theta_i,\theta_d)}{R''_{\nu ref}(\theta_i,\theta_d)} = \frac{d\Phi^{d}_{\nu samp}(\theta_i,\theta_d)}{d\Phi^{PD}_{\nu samp}(\theta_i,\theta_d)} \frac{d\Phi^{PD}_{\nu ref}(\theta_i,\theta_d)}{d\Phi^{d}_{\nu ref}(\theta_i,\theta_d)} \quad (3)$$

As $f(x,y)$ is assumed invariant during the experiments, the sum over A in Eq. (1) vanishes in the ratio $d\Phi^{d}_{\nu samp}/d\Phi^{d}_{\nu ref}$ of Eq. (3). For transmission measurements, $R''_{\nu samp}(\theta_i,\theta_d)$ is replaced by $T''_{\nu samp}(\theta_i,\theta_d)$ in Eq. (3).

3. Characterization of the mullite sample radiative properties

The aim of this section is to determine from reflectance and transmittance measurements the optical index n_S and the absorption and extinction coefficients $\kappa_{\nu S}$ and $\beta_{\nu S}$ of the solid mullite sample and to choose its scattering phase function $p_{\nu S}$. These determinations are carried out by identification between bi-directional transmittance and reflectance data issued from an adding doubling model and those issued from measurements.

3.1. Experimental results

Measurements in the incidence plane of the mullite sample bi-directional reflectance and transmittance defined in Section 2.2 have been carried out for three incidence angles θ_i (20°, 30°, 50°). It is worth of notice that, as shown in Fig. 2a, the reflectance presents, in the experimental range, both a quasi isotropic diffuse part and a specular peak. Still more singular features are that the diffuse reflectance is large, in the range [0.5;0.7] and the transmittance is very weak and quasi isotropic, close to 0.01. The typical measurement absolute fluctuations vary from 0.01 to 0.03 in the case of the reflectance and from 5×10^{-4} to 1×10^{-3} in the case of transmittance.

3.2. Radiative properties

Theoretically, the sample real optical index $n_{\nu S}$, extinction coefficient $\beta_{\nu S}$, albedo $\omega_{\nu S}$ and phase function $p_{\nu S}$ have to be determined from experimental data. The pointed out large optical thickness of the sample (26) is a strong limitation of an accurate determination of $p_{\nu S}$. The important diffuse part of the reflectance and the lack of collimated transmittance (Fig. 2) lead us to assume that the phase function is isotropic ($p_{\nu S}=1$). This hypothesis, which could be easily checked with smaller thickness samples, used in the determination of $\beta_{\nu S}$, $\omega_{\nu S}$, $n_{\nu S}$, will be discussed in the following.

In the model, it is also assumed that: (i) there is no time dependence; (ii) the geometry is a set of uniform layers of finite thickness and infinite extent in directions parallel to the surface; (iii) all the layers have the same uniform scattering and absorption coefficients and index of refraction; (iv) reflection and transmission at boundaries are governed by the Fresnel's laws; (v) light is not polarized; (vi) there is no internal source or emission. The bi-directional reflectance and transmittance R''_{ν} and T''_{ν} are calculated with an adding doubling method detailed in Refs. [17,18]. The identification of $n_{\nu S}$, $\beta_{\nu S}$ and $\omega_{\nu S}$ is carried out by an iterative procedure using the previous calculations and based on the minimization of a criterion given later. At the nth step, the albedo $\omega_{\nu S}$ and the index $n_{\nu S}$ are identified from the reflectance measurements, for the three considered incidence angles, by using the optical thickness value $\beta_{\nu S}d$ of the $(n-1)$th step. The optical thickness is then identified from the corresponding transmittance measurements with

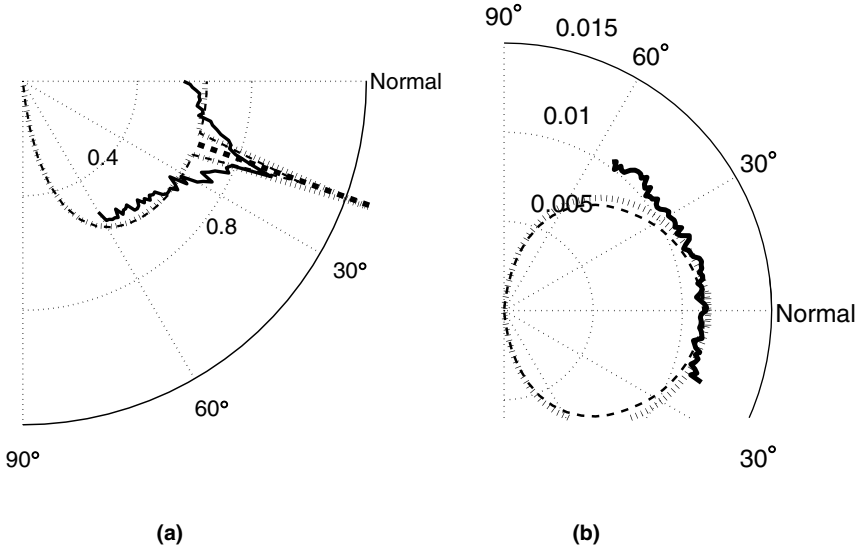

Fig. 2. Measured and calculated bi-directional reflectance (a) and transmittance (b) of the solid mullite sample vs θ_d, for $\theta_i=20°$ and $\lambda=0.6328$ nm; solid line: measurements; dashed lines: specific fit; other lines: global fit.

$\omega_{v\mathrm{S}}$ and $n_{v\mathrm{S}}$ values found previously. The identification is carried out until convergence. This procedure is initialized by considering an infinite optical thickness value.

The identification is based on the minimization of $V^2(\theta_i)$ defined by

$$V^2(\theta_i) = ([X_{\mathrm{exp}}(\theta_i) - X_{\mathrm{calc}}(\theta_i)]/X_{\mathrm{exp}}(\theta_i))^2 \quad (4)$$

where $X(\theta_i)$ is given, for reflection data, by

$$X(\theta_i) = \int_{\theta_{\mathrm{d\,min}}}^{\theta_{\mathrm{d\,max}}} R''_v(\theta_i, \theta_{\mathrm{d}}) \cos\theta_{\mathrm{d}}\, \mathrm{d}\Omega_{\mathrm{d}} \quad (5)$$

For transmission data $R''_v(\theta_i, \theta_{\mathrm{d}})$ is replaced by $T''_v(\theta_i, \theta_{\mathrm{d}})$. $[\theta_{\mathrm{d\ min}}, \theta_{\mathrm{d\ max}}]$ is the experimental range of reflectance (transmittance) measurements for a given θ_i. In Eq. (5), $X_{\mathrm{exp}}(\theta_i)$ and $X_{\mathrm{cal}}(\theta_i)$ are proportional to the experimental and calculated fluxes reflected in the incidence plane for the previously defined θ_{d} range. Identification results, related to $\omega_{v\mathrm{S}}$, $\beta_{v\mathrm{S}}d$ and $n_{v\mathrm{S}}$ are given in Fig. 3 with the minimal associated error V_0. For each identified value, an error bar is plotted; its boundaries correspond to the values of the considered quantity for which V is equal to two times its minimal value V_0. To complete this identification, a global fit have been carried out, from all the reflectance and transmittance measurements associated with the three incidence angles. The corresponding results, which are coherent with the previous results, are

$$\omega_{v\mathrm{S}} = 0.993, \quad \beta_{v\mathrm{S}} = 105\ \mathrm{mm}^{-1}, \quad n_{\mathrm{S}} = 1.48,$$
$$\kappa_{v\mathrm{S}} = 0.7\ \mathrm{mm}^{-1} \quad (6)$$

It is worth noticing that scattering is predominant and absorption is practically negligible, even if the absorption length is only of about 1 mm. The scattering length of about 10 μm is close to the typical 1 μm pore size.

An example of comparison of results issued from experiments and adding–doubling calculations is given in Fig. 2a and b. The global and the specific fits lead to similar results for reflectance which agree with experiments for the diffuse part of the reflectance. The specular reflectance is broadened by the effects of the sample roughness which is not taken into account in the model, as shown in Fig. 2a. This type of reflection can be associated with the difference between the measured and the calculated reflectance R''^{meas}_v and R''^{calc}_v from θ_A to θ_B. It is worth of notice that $2\pi \int_{\theta_A}^{\theta_B} (R''^{\mathrm{meas}}_v - R''^{\mathrm{calc}}_v) \cos\theta_{\mathrm{d}} \sin\theta_{\mathrm{d}}\, \mathrm{d}\theta_{\mathrm{d}}$ is then equal to the bi-directional specular reflectivity given by the model $\rho''_{v\ \mathrm{spec}}$, with a discrepancy of 0.009. The associated relative error is 0.09.

Transmittance discrepancies appear for θ_{d} higher than 25° between calculated and measured results. These discrepancies could be linked to surface roughness effects, which makes the transmittance higher for large θ_{d} values.

We have studied the sensitivity of the results to realistic values of the phase function $p_{v\mathrm{S}}$. Discrepancies on the diffuse part of the reflectance less than 0.03 and on the transmittance less than 0.001 as mentioned in Section 3.1 are considered. In this sensitivity study, $n_{v\mathrm{S}}$ and $\kappa_{v\mathrm{S}}$ have been taken equal to Eq. (6) values. Indeed, whatever $\beta_{v\mathrm{S}}$ value, the discrepancy on the reflectance is larger than 0.09 for $\kappa_{v\mathrm{S}} = 1\ \mathrm{mm}^{-1}$ (30% larger than the determined value). Let us recall that the absorption is here weak. We have arbitrary considered that $p_{v\mathrm{S}}$ is of the Heyney–Greenstein type, equal to $(1-g^2)/(1+g^2-2g\cos\theta)^{3/2}$ and studied its dependance on the scattering parameter g ($g = 0$ corresponds to the previously assumed isotropic phase function). In these conditions, it has been shown that the minimal acceptable value of g is -0.1 associated with $\beta_{v\mathrm{S}}d = 23.5$ and the maximal acceptable value of g is 0.2 associated with $\beta_{v\mathrm{S}}d = 29.5$. It is worth of notice that these two $\beta_{v\mathrm{S}}d$ values belong to the range studied in Fig. 3. In conclusion, the isotropic phase function, associated with $g = 0$ is in the center of acceptable range of g.

4. Validation case of the RDFI method

The aim of this section is to compare, for the considered foam sample, experimental bi-directional reflectance results obtained in Section 4.1 by the previously described technique with corresponding predicted results. These last results are obtained by a radiative Monte Carlo transfer model defined in Section 4.2 and applied to the equivalent semi transparent medium characterized by anisotropic radiative properties issued from the RDFI approach of Ref. [15]. It is a first validation case of the RDFI approach.

4.1. Measured porous mullite sample bi-directional reflectance

As the 12 mm sample thickness is much larger than its extinction length, transmission measurements cannot be carried out. It is, in practice, impossible to cut a small representative sample, which could allow us to undertake

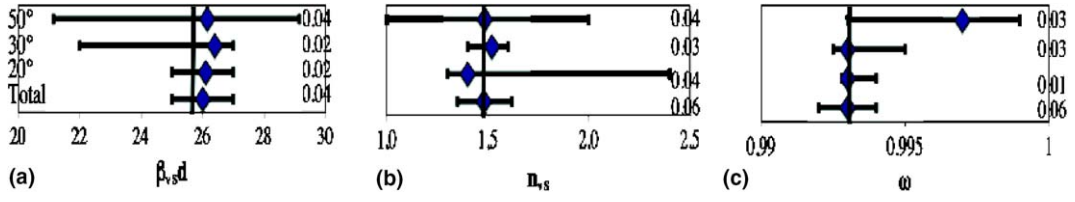

Fig. 3. Independent identification of (a) $\beta_{v\mathrm{S}}d$, (b) $n_{v\mathrm{S}}$ and (c) $\omega_{v\mathrm{S}}$ for given θ_i values (20°, 30°, 50°) and all θ_i values (total); the given data correspond to the minimal values of V_0; vertical lines correspond to the global fit.

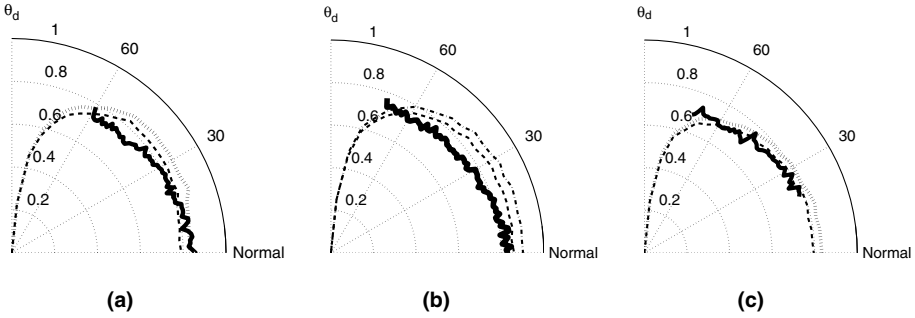

Fig. 4. Bi-directional reflectance data for the sensitivity study to $\beta_{v\mathrm{S}}$, $\omega_{v\mathrm{S}}$ and $n_{v\mathrm{S}}$ values for $\theta_i = $ (a) 20°, (b) 30° and (c) 50°; solid lines are experiments; dashed lines for Monte Carlo calculations (case 1) with $\beta_{v\mathrm{S}}d = 26.28$, $\omega_{v\mathrm{S}} = 0.9932$ and $n_{v\mathrm{S}} = 1.484$; dotted lines for Monte Carlo calculations (case 2) with $\beta_{v\mathrm{S}}d = 21$, $\omega_{v\mathrm{S}} = 0.988$ and $n_{v\mathrm{S}} = 1.32$.

these measurements. Experimental bi-directional reflectances data obtained by using the procedure defined in Section 2.3 are shown in Fig. 4a–c for three values of θ_i (20°, 30° and 50°) and a given range of θ_d in the incident plane.

4.2. Predicted porous mullite sample bi-directional reflectance

The mullite porous sample is considered as an anisotropic semi transparent medium; it is characterized by directional absorption and extinction coefficients $\kappa_v(\mathbf{u})$ and $\beta_v(\mathbf{u})$ and a real phase function $p_v(\mu_\mathrm{s})$ which has been found to depend only on the scattering angle μ_s [15]. But if this homogenized porous medium is represented by a plane layer, there is no physical plane interface i.e. no reflection and no transmission following the Descarte's laws at the interface. In this model, these phenomena have been accounted for in the equivalent semi transparent medium radiative properties.

A classical Monte Carlo transfer model is used to predict the bi-directional reflectance of the sample as explained for instance in [19]. The laser beam is modeled by a huge associated set of rays 2.5×10^8, with identical power bundles impacting the equivalent semi transparent medium with the incidence angles θ_i and ϕ_i corresponding to the laser beam direction $\mathbf{u}_i$ of the real case. The method is hybrid: (ii) scattering is stochastically modeled; (i) absorption is calculated in a deterministic way along a ray. This approach, based on the statistical independence of absorption and scattering, is justified in Refs. [20,21]. The stochastic calculation of scattering is based on the modeling of its cumulated distribution function, i.e. the associated transmissivity $\exp[-\sigma_v(\mathbf{u})d]$.

At the beginning of the calculation step i, the ray is defined, at the point M_i of abscissis s_i, by the angles θ_{i-1} and ϕ_{i-1} and characterized by the power P_{vi-1}. From a randomly generated number ξ_i, a scattering length d_i equal to $-\ln(\xi_i)/\sigma_v(\mathbf{u}_{i-1})$ is obtained. If the abscissis $s_{i+1} = s_i + d_i$ belongs to the material two phenomena occurred: (i) the bundle power P_{vi} becomes $P_{vi-1}\exp([-\kappa_v(\mathbf{u}_{i-1})d_i])$; (ii) the ray direction $\mathbf{u}_i$ is redefined by determining the new angles θ_i and ϕ_i from the generation of two random numbers $\xi_{i\theta}$ and $\xi_{i\phi}$ in the range $[0,1]$; ϕ_i is equal to $2\pi\xi_{i\phi}$; μ_s cosine of the scattering angle $\theta_i - \theta_{i_1}$ is defined from the equation involving its cumulated distribution function, i.e. $\xi_{i\theta} = \dfrac{\int_{-1}^{\mu_\mathrm{s}} p_v(\mu_\mathrm{s})\,\mathrm{d}\mu_\mathrm{s}}{\int_{-1}^{1} p_v(\mu_\mathrm{s})\,\mathrm{d}\mu_\mathrm{s}}$. If the point M_{i+1} of abscissis s_{i+1}, does not belong to the medium, there is no more scattering event. The ray impact I at the interface is determined and the distance M_iI replaces d_i in the calculation of the bundle power. This power is added to the reflected or transmitted directional flux in one of the 4050 solid angles of the calculation discretization. The relative standard deviation $\sigma_{\mathrm{MC}}(\theta_i)$ over the directional reflectance calculation is

$$\sigma_{\mathrm{MC}}(\theta_i) = \left\{ \frac{\sum_j [R''_{vk+1}(\theta_i,\theta_{\mathrm{d}j})\cos\theta_{\mathrm{d}j} - R''_{vk}(\theta_i,\theta_{\mathrm{d}j})\cos\theta_{\mathrm{d}j}]^2}{\sum_j [R''_{vk+1}(\theta_i,\theta_{\mathrm{d}j})\cos\theta_{\mathrm{d}j}]^2} \right\}^{1/2}, \tag{7}$$

where k deals with the successive sets of rays in the Monte Carlo calculation, the $k+1$th set of rays contains five times more rays than the kth set.

4.3. Comparison between measured and predicted bi-directional reflectance

The transfer model of Section 4.2 has been first carried out, for the porous mullite sample, with the directional radiative properties obtained by the RDFI approach [15] which requires itself the radiative properties of the solid phase (the solid sample of Section 3.2, case 1). In a first step, we have used the optimal results of Eq. (5) and the corresponding calculated $\beta_v(\mathbf{u})$, $\kappa_v(\mathbf{u})$ and $p_v(\mu_\mathrm{s})$ by the RDFI model. The Monte Carlo transfer model results are in rather good agreements with the experimental data as shown in Fig. 4a–c for the incidence angle $\theta_i = 20°$, 30°, 50°. In a second step, in order to refine the comparison another calculation has been carried out from other data for the solid sample, i.e. $\beta_{v\mathrm{S}}d = 21$, $\omega_{v\mathrm{S}} = 0.988$ and $n_{v\mathrm{S}} = 1.32$ (case 2). These new data correspond to a choice of results of Section 3.2 associated with V equal to two times its minimal value V_0. To make comparisons easier, these data have been chosen in order to obtain R''_v on the other side of the experimental curve.

The discrepancies between the experimental results and these calculated from Eq. (5) appear to be of the same order as the discrepancies between results issued from the two sets of data ($\beta_v(\mathbf{u})$, $\kappa_v(\mathbf{u})$ and $p_v(\mu_s)$), themselves issued from two sets of β_{vS}, ω_{vS} and n_{vS}.

The relative standard deviation associated with the Monte Carlo calculation, $\sigma_{MC}(\theta_i)$ defined in Eq. (7), is about 0.005 for 2.5×10^8 incident rays. The global relative error between experimental and calculation results defined as

$$\epsilon_r(\theta_i)=\frac{\sum_j \rho_v''^{\exp}(\theta_i,\theta_j)\cos(\theta_j)-\sum_j \rho_v''^{\mathrm{calc}}(\theta_i,\theta_j)\cos(\theta_j)}{\sum_j \rho_v''^{\exp}(\theta_i,\theta_j)\cos(\theta_j)} \tag{8}$$

is less than 0.07 and less than 0.12 for the first and second calculation set respectively. The agreement is rather good. It is worth noticing that the calculated results do not account for the different effects associated with the interface roughness in the initial determination of the basic data related to the solid phase: β_{vS}, ω_{vS} and n_{vS}.

5. Conclusion

We have first experimentally determined the absorption and extinction coefficients of a mullite sample. Scattering is preponderant characterized by an almost isotropic phase function. The experimental bi-directional reflectance of a foam sample, with a mullite solid phase previously studied, agrees with the theoretical reflectance obtained by the RDFI method of Zeghondy et al. [15]. It is a first validation of this approach.

Acknowledgement

The authors thank A. Tarrats (EM2C laboratory) for help during experiments.

References

[1] K. Kamiuto, A constrained least-squares method for limited inverse scattering problems, JQSRT 40 (1) (1988) 47–50.
[2] K. Kamiuto, M. Sato, M. Iwamoto, Determination of the radiative properties of high-porosity materials by use of the emerging-intensity fitting method, JQSRT 42 (6) (1989) 477–482.
[3] K. Kamiuto, Application of the emerging-intensity fitting method for inverse scattering problems to a system bounded by transparent plates, JQSRT 46 (3) (1991) 159–164.
[4] L. Glicksman, M. Shuetz, M. Sinofsky, Radiation heat transfer in foam insulation, Int. J. Heat Mass Transfer 30 (1) (1987) 187–197.
[5] T.J. Hendricks, J.R. Howell, Inverse radiative analysis to determine spectral radiative properties using the discrete ordinates method, in: G.F. Hewitt (Ed.), The Tenth International Heat Transfer Conference, vol. 2, Taylor and Francis, Brighton, UK, 1994, pp. 75–80.
[6] T.J. Hendricks, J.R. Howell, Absorption/scattering coefficients and scattering phase function in reticulated porous ceramics, ASME J. Heat Transfer 118 (1) (1996) 79–87.
[7] T.J. Hendricks, J.R. Howell, New radiative analysis approach for reticulated porous ceramics using discrete ordinates method, ASME J. Heat Transfer 118 (4) (1996) 911–917.
[8] D. Doermann, J.F. Sacadura, Heat transfer in open cell foam insulation, ASME J. Heat Transfer 118 (1996) 88–93.
[9] D. Baillis, M. Raynaud, J.F. Sacadura, Spectral radiative properties of open-cell foam insulation, J. Thermophys. Heat Transfer 13 (3) (1999) 292–298.
[10] R. Lopes, M. Luis, D. Baillis, J.F. Sacadura, Directional spectral emittance of a packed bed: correlation between theoretical prediction and experimental data, ASME J. Heat Transfer 123 (2001) 240–248.
[11] D. Baillis, J.F. Sacadura, Identification of polyurethane foam radiative properties—influence of transmittance measurements number, J. Thermophys. Heat Transfer 16 (2) (2002) 200–206.
[12] R. Viskanta, M.P. Mengüc, Radiative transfer in dispersed media, ASME, Appl. Mech. Rev. 42 (9) (1989) 241–259.
[13] D. Baillis, J.F. Sacadura, Thermal radiation properties of dispersed media: theoretical prediction and experimental characterization, JQSRT 67 (5) (2000) 327–363.
[14] M. Tancrez, J. Taine, Direct identification of absorption and scattering coefficients and phase function of a porous medium by a Monte Carlo technique, Int. J. Heat Mass Transfer 47 (2) (2004) 373–383.
[15] B. Zeghondy, E. Iacona, J. Taine, Determination of the anisotropic radiative properties of a porous material by radiative distribution function identification (RDFI), Int. J. Heat Mass Transfer, in press, doi:10.1016/j.ijheatmasstransfer.2006.02.034.
[16] J.J. Greffet, F.R. Ladan, Comparison between theoretical and experimental scattering of an S-polarized electromagnetic wave by a two-dimensional obstacle on a surface, J. Opt. Soc. Am. A 8 (8) (1991) 1261–1269.
[17] S. Chandrasekhar, Radiative Transfer, Dover Publications Inc., New York, 1960.
[18] R.M Goody, Y.L Yung, Atmospheric Radiation Theoretical Basis, second ed., Oxford University Press, 1989.
[19] R. Siegel, J. Howell, Thermal Radiation Heat Transfer, fourth ed., Taylor and Francis-Hemispher, Washington, 2001.
[20] J. Taine, J.P. Petit, Transferts thermiques: Introduction aux sciences des transferts, third ed., Dunod, Paris, 2003.
[21] L. Tessé, Modélisation des transferts radiatifs dans les flammes turbulentes par une méthode de Monte Carlo, Thèse de Doctorat, École Centrale Paris, Chatenay Malabry, 2001.